Discover Chemical Engineering

Discover

Research

Towards sustainable battery recycling: selective dynamic adsorption of nickel(II) and cobalt(II) in an adsorbent fixed-bed reactor at elevated temperature

Björn Robeck[1] · **Helena Horn**[1]

Received: 26 September 2023 / Accepted: 5 December 2023
Published online: 03 January 2024

Abstract
Caused by the scarce resources of critical heavy metals which are in high demand, e.g., for lithium-ion batteries, processes for the recovery of such materials for recycling are of high interest. Adsorption is an effective method in order to selectively separate metal ions from aqueous solutions. Unfortunately, the prerequisites in battery recycling, like acidic pH-value and high temperature, are in general impairing the adsorption process. In this study, the competitive dynamic adsorption of nickel(II) (Ni(II)) and cobalt(II) (Co(II)) by a silica adsorbent functionalized with amino-polycarboxylate derivative ligands (designated as HSU331) under recycling process conditions, (pH = 3.5, T = 20 °C, and T = 50 °C, respectively) and varying concentrations (Ni(II):Co(II) 1:1 (5.0, and 10 mmol·L^{-1}, respectively), Ni(II):Co(II) 3:1 and 1:3 (3.0 mmol·L^{-1} and 1.0 mmol·L^{-1} vice versa)) were investigated. A displacement desorption of Co(II) in favor of the binding of Ni(II) was observed, achieving maximum loadings of 0.95 $\mu mol_{Ni(II)} \cdot \mu mol_{Ligand}^{-1}$ (28.3 $mg_{Ni(II)} \cdot g_{Adsorbent}^{-1}$), and 0.48 $\mu mol_{Co(II)} \cdot \mu mol_{Ligand}^{-1}$ (14.3 $mg_{Co(II)} \cdot g_{Adsorbent}^{-1}$) at T = 20 °C and 1.0 $\mu mol_{Ni(II)} \cdot \mu mol_{Ligand}^{-1}$ (29.9 $mg_{Ni(II)} \cdot g_{Adsorbent}^{-1}$) and 0.18 $\mu mol_{Co(II)} \cdot \mu mol_{Ligand}^{-1}$ (5.38 $mg_{Co(II)} \cdot g_{Adsorbent}^{-1}$) at T = 50 °C, respectively. These results demonstrate a distinctly selective separation of Ni(II) in the presence of Co(II) by HSU331, achieving an even higher efficiency at elevated temperatures.

Keywords Heavy metal separation · Amino-polycarboxylate-functionalized Silica · Continuous adsorption · Diffusion · Breakthrough curve

1 Introduction

Separation of nickel (Ni) and cobalt (Co) from process waters is becoming increasingly important especially in battery recycling processes. This is caused inter alia by the growing global demand for electrochemical energy storage by lithium batteries (LIB) [1]. The most common combinations for LIB are lithium-nickel–cobalt-aluminum-oxide (NCA) and lithium-nickel-manganese-cobalt-oxide batteries (NMC) [1, 2].

An essential process of battery recycling are hydrometallurgical processes in order to remove Ni and Co, starting with acid leach [1, 3, 4]. After leaching, the metal ions exist as Ni(II) and (after subsequent reduction) as Co(II) in the acidic aqueous phase [3]. They can be recovered by precipitation, flocculation and solvent extraction [1, 3–8]. In order to increase the efficiency of established wastewater treatment processes, selective adsorption could be a suitable additional sub-process. Adsorption is characterized in terms of operating cost, selectivity towards specific target components, and

✉ Björn Robeck, robeckb@hsu-hh.de; Helena Horn, helena.horn@hsu-hh.de | [1]Institute of Thermodynamics, Helmut-Schmidt-University/University of the Bundeswehr Hamburg, Holstenhofweg 85, 22043 Hamburg, Germany.

efficient separation at low concentrations [9–12]. Concerning the possibilities for separate recovery of Ni(II) and Co(II), the application of highly selective adsorbents is required [9–12]. These can be produced by surface modification of the adsorbents with target-directed ligands [12–14]. Several studies have already shown the general possibility to bind Ni(II) and Co(II) by such adsorbents in batch experiments [10, 11, 14–19]. These discontinuous investigations of the adsorbents deliver valuable information about the adsorption equilibria and the microkinetics of the respective adsorption process. However, they can also lead to erroneous interpretations, if they are not supplemented by continuous experiments. Designing a selective adsorption-based separation process, a thorough assessment of an adsorbent additionally requires dynamic adsorption experiments (continuous mode) in order to determine the influence of convection and diffusion (macrokinetics) on mass transfer. The latter parameters are of great importance for the control and design of adsorbers when implementing the process in real applications [20, 21]. Moreover, the characteristics of the adsorption process might differ when comparing the two types of evaluation. In batch mode, the concentration of the target compound in the solution decreases over time, whereas in continuous experiments the concentration is steady, which might influence the adsorption equilibrium and therefore the maximum load of the adsorbents. Another benefit, especially when evaluating phenomena of competitive adsorption is, that more detailed information about the singular steps of binding and displacement of the target compounds can be generated.

In this study, we investigated the effect of temperature on the mass transfer and the residence time behavior in the column. Further, we examined the separation of Ni(II) and Co(II) from acidic aqueous solution in continuous dynamic experiments by silica functionalized with an amino-polycarboxylate derivative. This adsorbent, named HSU331, showed high adsorption capacities and a strong selectivity towards Ni(II) in previous batch experiments [22]. Since macrokinetics can be influenced by feed concentration as well as temperature, we compared the process varying the concentrations of the target substances and process temperature.

We evaluated if the selectivity of the adsorbent HSU331 towards Ni(II) can be confirmed in dynamic operation. Furthermore, the dependency of the breakthrough times on the operating temperature (T = 20 °C, and T = 50 °C, respectively) as well as the starting concentrations of the target compounds Co(II) and Ni(II) were investigated in equimolar as well as in proportions of 3:1 Co(II):Ni(II). Additionally, parameters such as adsorption capacity and bed volumes (BV) for pilot or operational scale-up are presented.

2 Experimental

For the experimental evaluations a model reactor was designed, the respective flow diagram is shown in Fig. 1. A TU peristaltic pump (Medorex, Bovenden, Germany) (2) conveyed the heavy metal solution (green) from the storage tank (1) into a Chromabond adsorption column (Macherey–Nagel, Düren, Germany) (3) at a flow rate of $\dot{v} = 1.0$ mL·min^{-1}. Samples were taken into Safe-Lock Tubes (Eppendorf, Hamburg, Germany) (4). The experimental temperature was regulated by a connected circuit (red) in which ultrapure water was heated by a UR-030-SH heater (ATP Messtechnik GmbH, Ettenheim,

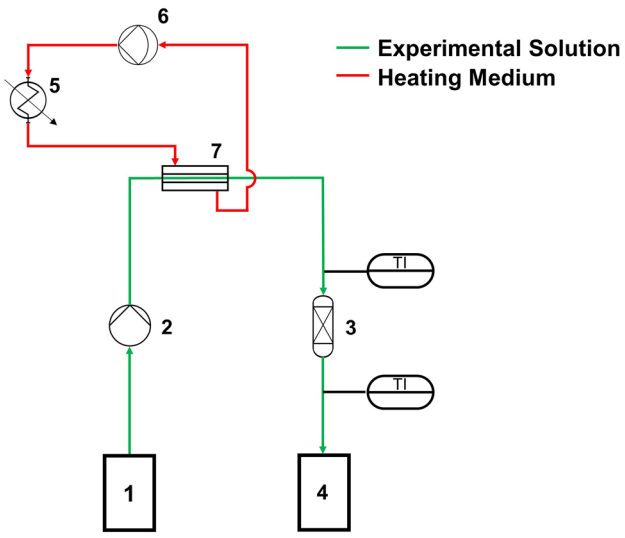

Fig. 1 Flow diagram of the adsorption column plant: storage tank (1), dosing pump (2), adsorption column with thermometers (3), sampling (4), heater (5), diaphragm pump (6), tube heat exchanger (7)

Germany) (5) and pumped by a NF 100 KT 18 diaphragm pump (KNF Liquiport, Sursee, Switzerland) (6) through a tube heat exchanger (7). The temperature was measured at the inlet as well as at the outlet of the column.

In order to generate reproducible fixed beds, the empty columns (3) were initially filled with 1.50 mL of ultrapure water, subsequently the adsorbents were filled in (0.57 g dry weight), corresponding to a bed height of 10 mm in the absorber column (average column diameter = 12.4 mm).

All described experiments were performed in triplicate at T = 20 °C, and T = 50 °C, respectively. All solutions applied were prepared using ultrapure water of type 1 provided by PURELAB Quest UV (Veolia, Celle, Germany).

At first, a test series in order to determine the flow behavior of the carrier solution and the residence time behavior of the reactor was done according to [20, 23]. For these investigations the unfunctionalized silica matrix of HSU331 (irregular particles, size: 40 – 64 µm, pore diameter: 60 Å) was employed. A 1 M solution of sodium chloride (NaCl) (purity > 99.5%; Merck, Darmstadt, Germany) with an electrical conductivity of 83 $mS{\cdot}cm^{-1}$ was utilized as a tracer, using the conductivity of the solution as surrogate parameter for the concentration. A step signal was applied to the system by inserting the chromabond column, causing an abrupt change to the tracer concentration at time $t = 0$ at the inlet. At the outlet, solution samples were collected in 0 – 30 s fractions and the conductivity was measured with a Lab 875 conductivity meter (SI-Analytics, Weilheim, Germany) in order to determine the step response and thus the residence time behavior of the system.

For the dynamic adsorption experiments, HSU331, a silica based adsorbent functionalized with an amino-polycarboxylate ligand, was employed. The functionalization (surface coverage) of the ligand amounts to 524 $\mu mol_{Ligand}{\cdot}g_{Adsorbent}{}^{-1}$, the pore diameter is 60 Å and the particle size 40 – 63 µm. The characterization of the adsorbent HSU331 in discontinuous batch experiments was previously performed by Kriese et al. [22].

As adsorptives, Co(II) nitrate hexahydrate ($Co(NO_3)_2{\cdot}(H_2O)_6$, purity > 98%) obtained from Carl Roth (Karlsruhe, Germany) and Nickel(II) nitrate hexahydrate ($Ni(NO_3)_2{\cdot}(H_2O)_6$, purity 99%) provided by Merck (Darmstadt, Germany) were applied. The pH value of the solutions was adjusted to pH = 3.5 utilizing nitric acid (65 wt%, Suprapur, Merck, Darmstadt, Germany).

The investigations were performed applying equimolar solutions of Ni(II):Co(II), comparing initial concentrations of $c_{01} = 5.0\ mmol{\cdot}L^{-1}$ and $c_{02} = 10\ mmol{\cdot}L^{-1}$ and for molar ratios of Ni(II):Co(II) 3:1 and 1:3, respectively. For the latter investigations, the concentration of the excess component amounted to 3.0 $mmol{\cdot}L^{-1}$, while the concentration of the minor component amounted to 1.0 $mmol{\cdot}L^{-1}$. Due to the strong influences of temperature (T = 20 °C – T = 90 °C) [24, 25], concentration of acid [1, 26] and time [1] in the leaching process, it is not yet possible to derive the final concentrations of the respective heavy metals from literature. Consequently, this study is designed as a proof of concept for the application of the presented method in leaching and hydrometallurgical process in battery recycling.

At the outlet of the column, solution samples were collected in 1 min fractions. The concentrations of Ni(II) and Co(II) in the samples were determined with an Inductively Coupled Plasma Mass Spectrometry (ICP-MS) on an Agilent 7800 instrument with the Autosampler SPS 4 from Agilent Technologies (Santa Clara, CA, USA) according to Kriese et al. [27].

The observation time of the experiments in all cases started as soon as the solution first came into contact with the column. Because of the volume of the adsorbents (1.0 cm^3) and the flow rate of the fluid solution (1.0 $mL{\cdot}min^{-1}$) the experimental time also refers to the dimensionless bed volumes (BV), which is defined as the volume ratio of the effluent to the volume of the adsorption bed. In total, the experimental time was 10.0 min for the determination of the residence time behavior, 180 min for the investigation of the competitive adsorption with molar ratios of 1:1 and 3:1 (Ni(II):Co(II)), and 360 min for the molar ratio 1:3 (Ni(II):Co(II)), respectively.

3 Results and Discussion

In the following section, the analysis of the residence time behavior in the adsorbent column and the breakthrough profiles of Ni(II) and Co(II) are presented.

3.1 Residence time behavior

In order to investigate the residence time behavior of the continuous flow reactor, the residence time sum function $F(t)$ (Eq. 1), the residence time density function $E(t)$ (Eq. 2) and the average residence time $\bar{t}$ (Eq. 3) were calculated as described below [20, 23] using the measured conductivities Υ at the outlet of the column.

$$F(\mathrm{t}) = c(\mathrm{t}) \cdot c_0^{-1} = \gamma(t) \cdot \gamma_0^{-1} \tag{1}$$

$$E(\mathrm{t})\,\mathrm{dt} = \mathrm{d}F(\mathrm{t}) \tag{2}$$

$$\bar{t} = \int_0^{\infty} t \cdot E(t) dt \tag{3}$$

The degree of axial mixing was calculated by the axial dispersion coefficient D_{ax} according to Eq. 4 where u is the flow velocity, L the length (bed height), and Bo the Bodenstein-number.

$$D_{ax} = (u \cdot L) \cdot Bo^{-1} \tag{4}$$

The Bodenstein-number characterizes the back-mixing and is determined according to Eq. 5 where ε is the bed porosity and Re the Reynolds-number [20, 28].

$$Bo = 0,2 \cdot \varepsilon^{-1} + (0,011 \cdot Re^{0,48}) \cdot \varepsilon^{-1} \tag{5}$$

The Reynolds number is a dimensionless ratio number and indicates the flow conditions in the flow tube according to Eq. 6.

$$Re = u \cdot d \cdot v^{-1} \tag{6}$$

where the flow velocity u is multiplied by the characteristic length d of the tube divided by the kinematic viscosity v. Furthermore, the particle Reynolds number according to Eq. 7 describes the flow conditions around the particles in the packed bed column.

$$Re_p = u \cdot d_p \cdot v^{-1} \tag{7}$$

Herein d_p describes the average grain diameter of the particle.

In addition to the flow conditions in the column, diffusion processes have a decisive influence on the mass transport to the surface of solids. The influence of diffusion on mass transport in the pores of silica can be determined by the effective diffusion coefficient of hydrated molecules in aqueous solution. This parameter describes the deviation of pore diffusion from free diffusion. For this purpose, the binary diffusion coefficient of hydrated molecules in the liquid phase must be determined. Assuming spherical molecules, the binary diffusion coefficient D_{12} can be described by the Stokes–Einstein equation (Eq. 8), where k_B is the Boltzmann constant ($k_B = 1.38 \cdot 10^{-23}$ J·K^{-1}), T the Temperature in Kelvin, η the solvent viscosity and R_o the solute ratio [29].

$$D_{12} = (k_B \cdot T) \cdot (6 \cdot \pi \cdot \eta \cdot R_o)^{-1} \tag{8}$$

With the particle porosity ε_P and the tortuosity factor τ, the effective diffusion coefficient D_{eff} can be estimated using Fick's first law (Eq. 9).

$$D_{eff} = \varepsilon_P \cdot D_{12} \cdot \tau^{-1} \tag{9}$$

The particle porosity ε_P can be calculated via the pore volume of the solid material [20]. According to Probst [30], $\tau = 1.8$ can be assumed as a representative value for silica gels.

The ascertained parameters are summarized in Table 1. The diffusion coefficients for Na^+ and Cl^- in the dilute solution presented in here were taken from Cussler and Boudreau [29, 31] (given at a temperature of T = 25 °C in the range of 10^{-9} m^2·s^{-1}) and adjusted according to the temperature applying the Stokes Einstein equation (Eq. 8).

The increased temperature causes a decrease of the fluid viscosity. Thus, the laminar boundary layer around the adsorbent particles (Re_p), the binary diffusion coefficient D_{12} and the effective diffusion coefficient D_{eff} of hydrated Na^+ and Cl^- are approximately halved at a temperature of T = 50 °C in comparison to T = 20 °C (see Table 1). The temperature has no significant impact on the backmixing (D_{ax}) inside the packed column in axial direction, consequently this can be excluded as a cause for the elongated residence times ($D_{axSilica\ 20\ °C} = 2.75 \cdot 10^{-8}$ m^2·s^{-1} and $D_{axSilica\ 50\ °C} = 2.74 \cdot 10^{-8}$ m^2·s^{-1}).

Table 1 Average residence time, Reynolds numbers, and diffusion coefficient depending on temperature (20 °C | 50 °C) and column filling (1.5 mL ultrapure water | 0.57 g unfunctionalized Silica)

column filling	T/°C	average residence time $\bar{t}$/min	*Re*, Re_p resp.	$D_{12}Na^+/m^2 \cdot s^{-1}$	$D_{12}Cl^-/m^2 \cdot s^{-1}$	$D_{eff}Na^+/m^2 \cdot s^{-1}$	$D_{eff}Cl^-/m^2 \cdot s^{-1}$
Water	20	1.49	1.71*				
Water	50	1.28	3.09*				
Silica	20	2.90	$7.09 \cdot 10^{-3}$**	$1.17 \cdot 10^{-9}$	$1.78 \cdot 10^{-9}$	$3.18 \cdot 10^{-10}$	$4.81 \cdot 10^{-10}$
Silica	50	2.57	$1.29 \cdot 10^{-2}$**	$2.37 \cdot 10^{-9}$	$3.59 \cdot 10^{-9}$	$6.43 \cdot 10^{-10}$	$9.74 \cdot 10^{-10}$

* *Re* ** Re_p

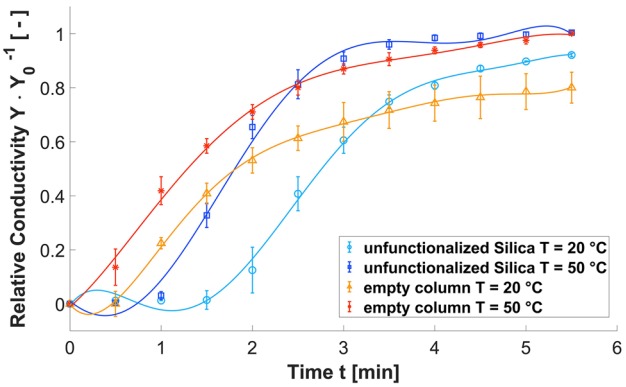

Fig. 2 Residence time sum function *F(t)*; $\dot{v} = 1.0$ mL·min^{-1}, feed concentration $c_0 = 1$ M NaCl solution onto 1.5 mL filled ultrapure water column (empty column), and onto a column filled with unfunctionalized silica material, respectively

The sum functions *F(t)* are presented in Fig. 2. On the ordinate, the relative conductivity $\gamma \cdot \gamma_0^{-1}$ at the column outlet and on the abscissa the experimental time are presented. The NaCl solution broke through after 1.0 min at T = 50 °C, and after 1.5 min at T = 20 °C. After 4.0 min at T = 50 °C and after 5.0 min at T = 20 °C, 90% of the initial input conductivity was measured at the outlet.

In the column filled with unfunctionalized carrier material the average residence time $\bar{t}$ amounted to 2.9 min at T = 20 °C and 2.6 min at a temperature of T = 50 °C.

This results in an increase of residence time due to the adsorbents with $\Delta t_{20°} = 1.4$ min and $\Delta t_{50°} = 1.3$ min. Both values describe the time during which the adsorbent is in direct contact with the target compounds in the fluid phase. Thus, the average contact time decreased with increased temperature, which is generally disadvantageous for adsorption. This can be explained by the decrease in viscosity with higher temperature. At a temperature of T = 20 °C, 1 M NaCl has a dynamic viscosity of $\eta_{NaCl\ 20\ °C} = 1.09$ mPa·s. In contrast, the viscosity of $\eta_{NaCl\ 50\ °C} = 0.61$ mPa·s at T = 50 °C is almost halved [32]. This behavior is also shown by water. Here, the dynamic viscosity decreases from η_{H_2O} 20 °C = 1.00 mPa·s. at T = 20 °C to η_{H_2O} 50 °C = 0.55 mPa·s at T = 50 °C [33]. Therefore, we assume that this explanation also applies to the subsequent competitive adsorption experiments.

3.2 Influence of concentration and temperature on the competitive adsorption of Ni(II) and Co(II)

Adsorption describes the binding of a target substance (adsorptive) on the adsorbent surface of solid materials, such as silica gel. Energy is released in the form of (adsorption) heat. The adsorption of divalent metal ions (M(II)) on ligands (L) of the functionalized surface of an adsorbent proceeds according to the equilibrium reaction described by Eq. 10.

$$L + M(II) \rightleftharpoons L - M(II) \tag{10}$$

In this process, the M(II) ions and the ligand *L* form a chemical complex. With the amount of material $n_{M(II)}$ of the adsorbed metal ion in $\mu mol_{M(II)}$ and the amount of material n_{Ligand} of the adsorbents in μmol_{Ligand}, which is composed of the mass of the adsorbent $m_{Adsorbents}$ and the degree of functionalization *F*, the adsorption loading *q* for a single fraction of dynamic adsorption was determined according to Eqs. 11 and 12 in $\mu mol_{M(II)} \cdot \mu mol_{Ligand}^{-1}$.

$$n_{\text{Ligand}} = m_{\text{Adsorbents}} \cdot F \tag{11}$$

$$q = n_{\text{M(II)}} \cdot n_{\text{Ligand}}^{-1} \tag{12}$$

The breakthrough profiles of the competitive adsorption of Ni(II) and Co(II) onto the packed HSU331 adsorbents at T = 20 °C, and T = 50 °C, respectively, are presented in Figs. 3 and 4. On the ordinate, the relative concentration $c_t \cdot c_0^{-1}$ at the column outlet and on the abscissa the experimental time is presented. Figure 3. shows breakthrough profiles at HSU331 at T = 20 °C as well as at T = 50 °C regarding the dual-component solutions Ni(II) and Co(II) with equal concentrations (equimolarity 1:1) of 5.0 (Fig. 3a), and 10 mmol·L^{-1} (Fig. 3b), respectively. The obtained results according to Eqs. 11 and 12 are summarized in Table 2. Regarding the adsorption process at a temperature of T = 20 °C, the breakthrough times of Ni(II) and Co(II) were identical depending on the feed concentration: at 5.0 mmol·L^{-1} the breakthrough time of Ni(II) as well as of Co(II) was 14 min, at 10 mmol·L^{-1} it decreased for both substances to 7 min. At the process time of each breakthrough, almost 50% of the ligands of the adsorbent HSU331 were loaded. After 32 min at a concentration of 5 mmol·L^{-1}, and after 25 min at a feed concentration of 10 mmol·L^{-1}, respectively, about 90% of the ligands of the adsorbent HSU331 were occupied and a displacement desorption of Co(II) occurred. Thus, the effluent concentration of Co(II) was higher than the feed concentration. Presumably, the Co(II)/HSU331 ligand complexes were dissolved in favor of the formation of more stable Ni(II)/HSU331 ligand complexes [17, 22]. A similar behavior in an adsorbent fixed bed was found by Inoue et al., who demonstrated high adsorption capacity of functionalized chitosan with amino-polycarboxylic acids in continuous experiments targeting Ni(II) and Co(II) [34].

Due to the displacement of Co(II), the selectivity of the ligands towards Ni(II) is evident. This phenomenon can be explained by results of prior discontinuous studies regarding the thermodynamic characteristics of the complexation reactions. The complexation of Ni(II) by the ligand exhibits negative free enthalpies at T = 20 °C (ΔG = -17.3 kJ·mol^{-1}) as well as at T = 50 °C (ΔG = -17.7 kJ·mol^{-1}). The complexation of Co(II) by the ligand on the other hand, shows still negative, but higher free enthalpies at T = 20 °C (ΔG = -12.9 kJ·mol^{-1}) as well as at T = 50 °C (ΔG = -14.4 kJ·mol^{-1}). This indicates an elevated spontaneous nature of the Ni(II) complexation [22].

Similarly, two breakthrough times for Ni(II) and Co(II) were observed in the experiments at T = 50 °C. The breakthrough of Co(II) took place after the same retention times (14 min at 5.0 mmol·L^{-1} and 7 min at 10 mmol·L^{-1}) as in the experiments

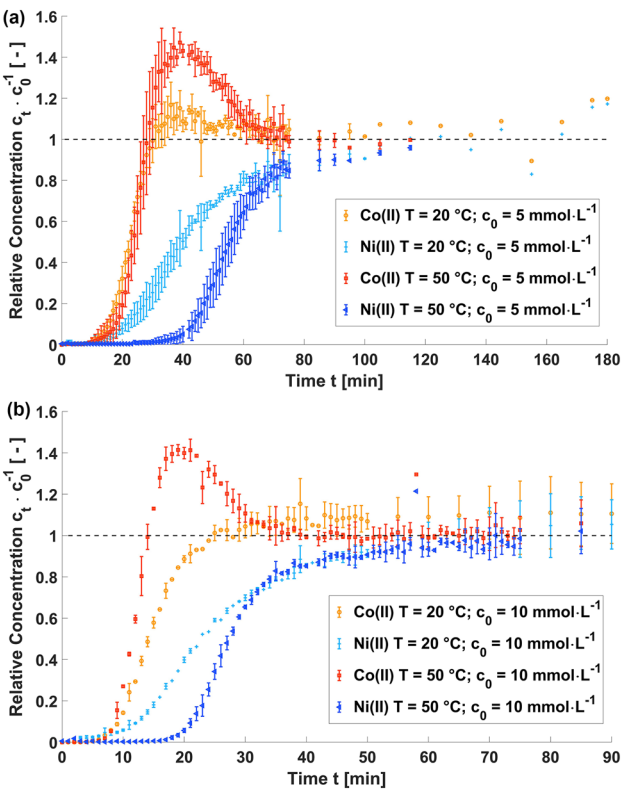

Fig. 3 Breakthrough profiles of Ni(II) and Co(II) onto 0.57 g HSU331, $\dot{v}$ = 1 mL·min^{-1} and pH = 3.5. **a** Feed concentration c_0 = 5 mM$_{\text{Ni(II)}}$ | 5 mM$_{\text{Co(II)}}$, T = 20 °C and T = 50 °C. **b** Feed concentration c_0 = 10 mM$_{\text{Ni(II)}}$ | 10 mM$_{\text{Co(II)}}$, T = 20 °C and T = 50 °C

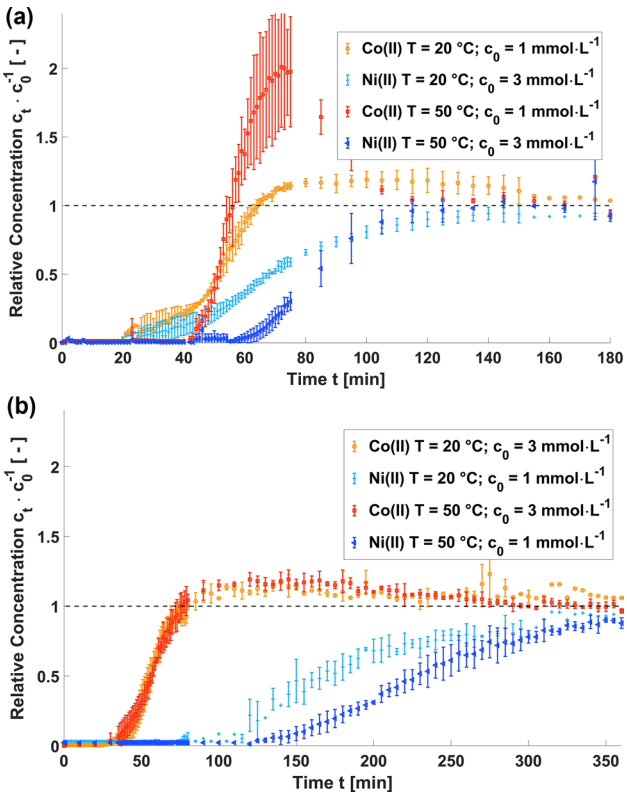

Fig. 4 Breakthrough profiles of Ni(II) and Co(II) onto 0.57 g HSU331, $\dot{v} = 1$ mL·min^{-1} and pH = 3.5. **a** Feed concentration $c_0 = 3$ $mM_{Ni(II)}$ | 1 $mM_{Co(II)}$, T = 20 °C and T = 50 °C. **b** Feed concentration $c_0 = 1$ $mM_{Ni(II)}$ | 3 $mM_{Co(II)}$, T = 20 °C and T = 50 °C

Table 2 Results of the breakthrough behavior onto 0.57 g HSU331, $\dot{v} = 1$ mL·min^{-1} and pH = 3.5, for feed concentration $c_0 = 5$ $mM_{Ni(II)}$ | 5 $mM_{Co(II)}$, and $c_0 = 10$ $mM_{Ni(II)}$ | 10 $mM_{Co(II)}$, T = 20 °C and T = 50 °C

$c_{0M(II)}$/mmol·L^{-1}	Adsorptive	T/°C	$n_{M(II)}$/µmol$_{M(II)}$	q/ µmol$_{M(II)}$·µmol$_{Ligand}^{-1}$
5	Ni(II)	20	187	0.61
	Co(II)		69.7	0.23
	Ni(II)	50	232	0.78
	Co(II)		56.6	0.19
10	Ni(II)	20	285	0.95
	Co(II)		144	0.48
	Ni(II)	50	306	1.02
	Co(II)		51.7	0.17

at T = 20 °C but the curve shows a much steeper slope, especially at the feed concentration of 10 mmol·L^{-1}, caused by a higher adsorption rate. At this time, 50% of the ligands of the adsorbent HSU331 were loaded. After 27 min at a concentration of 5 mmol·L^{-1}, and after 14 min at a feed concentration of 10 mmol·L^{-1}, respectively, about 90% of the ligands of the adsorbent HSU331 were occupied. Analogous to the results of the experiments at T = 20 °C, Co(II) bonded weaker and a displacement desorption occurred, presumably because of the different complex stabilities. In literature, higher complex stabilities for Ni(II) than for Co(II) are explained by higher ligand field stabilization energy (LFSE) for Ni(II) in coordination with oxygen or nitrogenous ligands [35]. This results in different equilibrium constants K_{ML} between Ni(II) and Co(II) (lg K_{ML}(Ni(II)/HSU331) = 3.32 and lg K_{ML}(Co(II)/HSU331) = 1.68, according to Kriese et al. [22] in competitive adsorption). Consequently, the outlet concentration of Co(II) exceeded the feed concentration ($c_t \cdot c_0^{-1} > 1$). After 85 min at a concentration of 5 mmol·L^{-1}, and after 40 min at feed concentration of 10 mmol·L^{-1}, respectively, the outlet concentration of Ni(II) reached 90% of the feed concentration.

Overall, the loading of Ni(II) and Co(II) in the equimolar solution with a concentration of 5 mmol·L^{-1} was lower because the adsorptiv to ligand ratio, and the concentration gradient, respectively, was lower than in the experiments with increased heavy metal concentration of 10 mmol·L^{-1}. Due to the structural formula of the ligand, more than one

Ni(II) per ligand can be bond at an increased concentration of 10 $mmol_{Ni(II)}·L^{-1}$. Kriese et al. [22] showed in competitive discontinuous batch adsorption experiments with an equimolar concentration of 5.6 $mmol·L^{-1}$ Ni(II) and Co(II) a max loading q^* of 0.54 $\mu mol_{Ni(II)}·\mu mol_{Ligand}^{-1}$ and 0.07 $\mu mol_{Co(II)}·\mu mol_{Ligand}^{-1}$ at 20 °C, and 0.51 $\mu mol_{Ni(II)}·\mu mol_{Ligand}^{-1}$ and 0.01 $\mu mol_{Co(II)}·\mu mol_{Ligand}^{-1}$ at 50 °C, respectively. Similar maximum loadings q^* were obtained at an initial concentration of 11 $mmol·L^{-1}$: 0.59 $\mu mol_{Ni(II)}·\mu mol_{Ligand}^{-1}$ and 0.05 $\mu mol_{Co(II)}·\mu mol_{Ligand}^{-1}$ at 20 °C, and 0.64 $\mu mol_{Ni(II)}·\mu mol_{Ligand}^{-1}$ and 0.09 $\mu mol_{Co(II)}·\mu mol_{Ligand}^{-1}$ at 50 °C, respectively.

In dynamic adsorption experiments, higher loadings than in batch experiments are possible, since metal solution is constantly added to the adsorbent at the initial concentration and thus the concentration gradient is always very high [36–38]. Consequently, the adsorptive to ligand ratio is higher than in the equilibrium batch experiments. At both temperatures, a displacement desorption of Co(II) was observed, but at a temperature of T = 50 °C the phenomenon was more pronounced.

The results show that at equal concentrations of Ni(II) and Co(II), the temperature had a minor influence on the loading of Ni(II). However, a significantly lower loading of Co(II) was obtained at a temperature of T = 50 °C onto HSU331. It can be assumed that the faster displacement desorption of Co(II) observed in our study was caused by a higher diffusion rate and consequently enhanced mass transfer in the pores of the adsorbent at T = 50 °C.

The experiments described so far were concerned with the simultaneous separation of Ni(II) and Co(II) present in equal concentrations in the feed solution. In the following section, the results of the separation process utilizing unequal molar ratios of the target compounds are presented. The breakthrough profiles on HSU331 at T = 20 °C and T = 50 °C are depicted in Fig. 4 regarding the molar ratios of 3:1 (3.0 $mmol·L^{-1}$ Ni(II), and 1.0 $mmol·L^{-1}$ Co(II)) (Fig. 4a), and 1:3 (1.0 $mmol·L^{-1}$ Ni(II) and 3.0 $mmol·L^{-1}$ Co(II)) (Fig. 4b), respectively. The obtained results according to Eq. 11 and Eq. 12 are summarized in Table 3.

The slope of the breakthrough curve of Co(II) at a molar ratio 3:1 at T = 20 °C starts to rise slightly after 20 min (28% of the ligands occupied). After 64 min (72% of the ligands occupied) the concentration at the adsorber outlet reached the inlet concentration of the feed solution. Since that moment, again the less stable Co(II)/HSU331 ligand complexes were resolved in favor of the formation of more stable Ni(II)/HSU331 ligand complexes, which is consistent with the results from the previous experiments. Ni(II) broke through simultaneously with Co(II) and the separation process was similar to the experiments with equal concentrations, but the breakthrough curve of Ni(II) was much flatter due to the lower concentration, which means that higher bed volumes were achieved. The outlet concentration of Ni(II) reached 90% of the inlet concentration after 110 min. At a molar ratio of 1:3, the surplus component Co(II) broke through after 31 min. After 75 min, Co(II) reached the inlet concentration. The same phenomena regarding Co(II) as in the previous experiments were observed. The minor component Ni(II) broke through after 110 min. The outlet concentration of Ni(II) reached 90% of the feed concentration after 310 min.

At T = 50 °C, at a molar ratio of 3:1, the steep increase of the Co(II) concentration started later, after 40 min (almost 50% of the ligands of the adsorbent HSU331 occupied), compared to T = 20 °C. The concentration of Ni(II) was also higher at T = 50 °C. A displacement desorption of Co(II) already took place after 56 min (80% of the ligands occupied). The released concentration of Co(II) reached the doubled amount of the input concentration.

Table 3 Results of the breakthrough behavior onto 0.57 g HSU331, $\dot{v} = 1$ $mL·min^{-1}$ and pH = 3.5, for feed concentration $c_0 = 3$ $mM_{Ni(II)}$ | 1 $mM_{Co(II)}$, and $c_0 = 1$ $mM_{Ni(II)}$ | 3 $mM_{Co(II)}$, T = 20 °C and T = 50 °C

$c_{0M(II)}$/$mmol·L^{-1}$	Adsorptive	T/°C	$n_{M(II)}$ /$\mu mol_{M(II)}$	q/ $\mu mol_{M(II)}·\mu mol_{Ligand}^{-1}$
3	Ni(II)	20	238	0.80
1	Co(II)		34.9	0.12
3	Ni(II)	50	276	0.92
1	Co(II)		24.1	0.08
1	Ni(II)	20	110	0.37
3	Co(II)		106	0.35
1	Ni(II)	50	181	0.60
3	Co(II)		85.8	0.29

After the beginning of the displacement desorption, consistently higher standard deviations of the measured Co(II) concentrations were observed (see Fig. 4a), which might be caused by a less homogeneous distribution of Co(II) inside the adsorbent pores under the given conditions (Ni(II):Co(II) 3:1).

The breakthrough curve of Ni(II) increased slowly after 60 min and 90% of the feed concentration were reached after 110 min. At a molar ratio of 1:3, Co(II) broke through at the same time as at a temperature of T = 20 °C, after 31 min the breakthrough curve rose steeply until it reached the input concentration after 75 min. Ni(II) was retained longer and broke through after 125 min.

The influence of the temperature on the breakthrough behavior is evident. The temperature had no influence on the loading height, but on the loading rate, which was significantly higher at T = 50 °C (see Figs. 3 and 4). The adsorption of Ni(II) and Co(II) took place simultaneously, until all ligands of the adsorbent HSU331 were occupied. Like in the previous experiments, the less stable Co(II)/HSU331 ligand complexes dissolved in favor of the formation of the more stable Ni(II)/HSU331 ligand complexes. The results demonstrate, that a small amount of Ni(II) in the presence of a large excess of Co(II) was successfully separated by dynamic adsorption onto HSU331, especially at T = 50 °C.

4 Conclusion

Applying the adsorbent HSU331 in continuous adsorption experiments at conditions which correspond to battery recycling processes (pH = 3.5, T = 20 °C, and T = 50 °C, respectively), high separation efficiencies of Ni(II) versus Co(II) were achieved (0.95 $\mu mol_{Ni(II)} \cdot \mu mol_{Ligand}^{-1}$ at T = 20 °C and 1.02 $\mu mol_{Ni(II)} \cdot \mu mol_{Ligand}^{-1}$ at T = 50 °C, 0.48 $\mu mol_{Co(II)} \cdot \mu mol_{Ligand}^{-1}$ at T = 20 °C and 0.18 $\mu mol_{Co(II)} \cdot \mu mol_{Ligand}^{-1}$ at T = 50 °C). This confirms similar results regarding HSU331 previously obtained in discontinuous studies [22] (0.54 $\mu mol_{Ni(II)} \cdot \mu mol_{Ligand}^{-1}$ at T = 20 °C and 0.51 $\mu mol_{Ni(II)} \cdot \mu mol_{Ligand}^{-1}$ at T = 50 °C, 0.07 $\mu mol_{Ni(II)} \cdot \mu mol_{Ligand}^{-1}$ at T = 20 °C and 0.01 $\mu mol_{Ni(II)} \cdot \mu mol_{Ligand}^{-1}$ at T = 50 °C). The selective separation of small amounts of Ni(II) in presence of a large excess of Co(II) was also successfully achieved by dynamic adsorption onto HSU331 (0.37 $\mu mol_{Ni(II)} \cdot \mu mol_{Ligand}^{-1}$ at T = 20 °C and 0.60 $\mu mol_{Ni(II)} \cdot \mu mol_{Ligand}^{-1}$ at T = 50 °C, 0.35 $\mu mol_{Co(II)} \cdot \mu mol_{Ligand}^{-1}$ at T = 20 °C and 0.29 $\mu mol_{Co(II)} \cdot \mu mol_{Ligand}^{-1}$ at T = 50 °C).

The selectivity mechanism was identified as displacement of the less stable Co(II)/HSU331 ligand complexes by Ni(II)/HSU331 ligand complexes. Similar phenomena were observed by Inoue et al. [34] when investigating functionalized chitosan with amino-polycarboxylic acids in continuous experiments targeting Ni(II) and Co(II).

Elevated temperature, and the resulting decreases of the residence time, respectively, had no influence on the loading height, but on the loading rate, which increased significantly at T = 50 °C.

The high loadings attained in all experiments demonstrate a high degree of utilization and thus a long service life of the adsorbent fixed bed. Consequently, so far, the adsorbent HSU331 seems suitable for application in industrial battery recycling process.

Author contributions All authors contributed to the manuscript

Funding Open Access funding enabled and organized by Projekt DEAL. The present work was partly financed by Ministry for Environment, Agriculture, Conservation and Consumer Protection of the State of North Rhine-Westphalia (MULNV). This publication has been funded by the Open-Access-Publication-Fund of the Helmut-Schmidt-University/University of the Bundeswehr Hamburg.

Data availability The experimental data used to support the findings of this study are available from the corresponding author upon reasonable request.

Declarations

Competing interests The authors declare no competing interests.

References

1. Windisch-Kern S, Gerold E, Nigl T, Jandric A, Altendorfer M, Rutrecht B, et al. Recycling chains for lithium-ion batteries: a critical examination of current challenges, opportunities and process dependencies. Waste Manag. 2022;138(1):125–39. https://doi.org/10.1016/j.wasman.2021.11.038.
2. Miao Y, Hynan P, von Jouanne A, Yokochi A. Current li-ion battery technologies in electric vehicles and opportunities for advancements. Energies. 2019. https://doi.org/10.3390/en12061074.
3. Zheng X, Zhu Z, Lin X, Zhang Y, He Y, Cao H, et al. A mini-review on metal recycling from spent lithium ion batteries. Engineering. 2018;4(3):361–70. https://doi.org/10.1016/j.eng.2018.05.018.
4. Joulié M, Laucournet R, Billy E. Hydrometallurgical process for the recovery of high value metals from spent lithium nickel cobalt aluminum oxide based lithium-ion batteries. J Power Sources. 2014;247(1):551–5. https://doi.org/10.1016/j.jpowsour.2013.08.128.
5. Yang Y, Yang Y, He C, Wei Y, Fujita T, Wang G, et al. Solvent extraction and separation of cobalt from leachate of spent lithium-ion battery cathodes with N263 in nitrite media. Int J Miner Metall Mater. 2023;30(5):897–907. https://doi.org/10.1007/s12613-022-2571-8.
6. Papadopoulos A, Fatta D, Parperis K, Mentzis A, Haralambous K-J, Loizidou M. Nickel uptake from a wastewater stream produced in a metal finishing industry by combination of ion-exchange and precipitation methods. Sep Purif Technol. 2004;39(3):181–8. https://doi.org/10.1016/j.seppur.2003.10.010.
7. Heredia JB, Martín JS. Removing heavy metals from polluted surface water with a tannin-based flocculant agent. J Hazard Mater. 2009;165(1–3):1215–8. https://doi.org/10.1016/j.jhazmat.2008.09.104.
8. Cheng CY, Barnard KR, Zhang W, Robinson DJ. Synergistic solvent extraction of nickel and cobalt: a review of recent developments. Solvent Extr Ion Exch. 2011;29(5–6):719–54. https://doi.org/10.1080/07366299.2011.595636.
9. Fu F, Wang Q. Removal of heavy metal ions from wastewaters: a review. J Environ Manag. 2011;92(3):407–18. https://doi.org/10.1016/j.jenvman.2010.11.011.
10. Ferri M, Campisi S, Gervasini A. Nickel and cobalt adsorption on hydroxyapatite: a study for the de-metalation of electronic industrial wastewaters. Adsorption. 2019;25(3):649–60. https://doi.org/10.1007/s10450-019-00066-w.
11. Awual R, Hasan M, Islam A, Asiri AM, Rahman MM. Optimization of an innovative composited material for effective monitoring and removal of cobalt (II) from wastewater. J Mol Liq. 2020;298:112035. https://doi.org/10.1016/j.molliq.2019.112035.
12. Awual R, Hasan M, Iqbal J, Islam A, Khandaker S, Asiri AM, et al. Ligand based sustainable composite material for sensitive nickel (II) capturing in aqueous media. J Environ Chem Eng. 2020;8(1): 103591. https://doi.org/10.1016/j.jece.2019.103591.
13. Thiesen PH, Niemeyer B. Maßgeschneiderte Adsorbentien im Anwendungsspektrum Bio- Medizin- und Umwelttechnik. Chem Ingenieur Tech. 2005;77(4):373–83. https://doi.org/10.1002/cite.200500003.
14. Piątek J, de Bruin-Dickason CN, Jaworski A, Chen J, Budnyak T, Slabon A. Glycine-functionalized silica as sorbent for cobalt (II) and nickel (II) recovery. Appl Surf Sci. 2020;530:147299. https://doi.org/10.1016/j.apsusc.2020.147299.
15. Yang P, Wang J, Wang S, Yang C, Zhao P, Huang B, et al. Study on the adsorption mechanism of cobalt and nickel in manganese sulfate by δ-MnO2. ACS Omega. 2022;7(42):37452–64. https://doi.org/10.1021/acsomega.2c04240.
16. Osińska M. Removal of lead (II), copper (II), cobalt (II) and nickel (II) Ions from aqueous solutions using carbon gels. J Sol-Gel Sci Technol. 2017;81(1):678–92. https://doi.org/10.1007/s10971-016-4256-0.
17. Repo E, Warchoł JK, Bhatnagar A, Sillanpää M. Heavy metals adsorption by novel EDTA-modified chitosan–silica hybrid materials. J Colloid Interface Sci. 2011;358(1):261–7. https://doi.org/10.1016/j.jcis.2011.02.059.
18. Tuomikoski S, Runtti H, Romar H, Lassi U, Kangas T. Multiple heavy metal removal simultaneously by a biomass-based porous carbon. Water Environ Res. 2021;93(8):1303–14. https://doi.org/10.1002/wer.1514.
19. Islam MA, Awual MR, Angove MJ. A review on nickel (II) adsorption in single and binary component systems and future path. J Environ Chem Eng. 2019. https://doi.org/10.1016/j.jece.2019.103305.
20. Baerns M, Hofmann H, Renken A. Chemische Reaktionstechnik (Lehrbuch der Technischen Chemie). 1st ed. Stuttgart: Thieme Verlag; 1987.
21. Bathen D, Breitbach M. Adsorptionstechnik. Berlin: Springer; 2013.
22. Kriese F, Lassen S, Niemeyer B. Recovery process for critical metals: selective adsorption of nickel (II) from cobalt (II) at acidic condition and elevated temperature. Adsorpt Sci Technol. 2023;2023(1):1–11. https://doi.org/10.1155/2023/5334353.
23. Levenspiel O. Chemical reaction engineering. 2nd ed. New York: John Wiley & Sons; 1998.
24. Li L, Dunn JB, Zhang XX, Gaines L, Chen RJ, Wu F, et al. Recovery of metals from spent lithium-ion batteries with organic acids as leaching reagents and environmental assessment. J Power Sources. 2013;233:180–9. https://doi.org/10.1016/j.jpowsour.2012.12.089.
25. Fan B, Chen X, Zhou T, Zhang J, Xu B. A Sustainable Process for the Recovery of Valuable Metals from Spent Lithium-ion Batteries. Waste Manag Res. 2016;34(5):474–81. https://doi.org/10.1177/0734242X16634454.
26. Meshram P, Pandey B, Mankhand T. Extraction of lithium from primary and secondary sources by pre-treatment, leaching and separation: a comprehensive review. Hydrometallurgy. 2014;150:192–208. https://doi.org/10.1016/j.hydromet.2014.10.012.
27. Kriese F, Lassen S, Horn H. A pitfall in heavy metal separation with amino-modified silica adsorbents from aqueous solution: the occurring pH shift. ChemistryOpen. 2022;11(5):1–8. https://doi.org/10.1002/open.202200034.
28. Müller-Erlwein E. Chemische Reaktionstechnik. 3rd ed. Wiesbaden: Springer-Verlag; 2015.
29. Cussler EL. Diffusion: mass transfer in fluid systems. 3rd ed. Cambridge, UK: Cambridge University Press; 2009.
30. Probst K, Wohlfahrt K. Empirische Abschätzung Effektiver Diffusionskoeffizienten in Porösen Systemen. Chem Ing Tec. 1979;51(7):737–9. https://doi.org/10.1002/cite.330510710.
31. Boudreau BP. Diagenetic models and their implementation. Berlin: Springer; 1997.
32. Kestin J, Khalifa HE, Correia RJ. Tables of the Dynamic and Kinematic Viscosity of Aqueous NaCl Solutions in the Temperature Range 20–150 °C and the Pressure Range 0.1–35 MPa. Journal of Physical and Chemical Reference Data. 1981;10(1):71–88. https://doi.org/10.1063/1.555641
33. Verein Deutscher Ingenieure. VDI-Wärmeatlas. 11th ed. Berlin: Springer; 2013.

34. Inoue K, Yoshizuka K, Ohto K. Adsorptive separation of some metal ions by complexing agent types of chemically modified chitosan. Anal Chim Acta. 1999;388(1–2):209–18. https://doi.org/10.1016/S0003-2670(99)00090-2.
35. Holleman AF. Lehrbuch der Anorganischen Chemie. Vol. 102, Walter de Gruyter; 2007.
36. Akratanakul S, Boersma L, Klock G. Sorption processes in soils as influenced by pore water velocity: 2. experimental results. Soil Sci. 1983;135(6):331–41. https://doi.org/10.1097/00010694-198306000-00001.
37. Gabriel U, Gaudet J-P, Spadini L, Charlet L. Reactive transport of uranyl in a goethite column: an experimental and modelling study. Chem Geol. 1998;151(1–4):107–28. https://doi.org/10.1016/S0009-2541(98)00074-6.
38. Limousin G, Gaudet J-P, Charlet L, Szenknect S, Barthes V, Krimissa M. Sorption isotherms: a review on physical bases modeling and measurement. Appl Geochem. 2007;22(2):249–75. https://doi.org/10.1016/j.apgeochem.2006.09.010.